Journal of Power Sources 248 (2014) 172–179

Contents lists available at ScienceDirect

Journal of Power Sources

journal homepage: www.elsevier.com/locate/jpowsour

Multiphysics modeling of lithium ion battery capacity fading process with solid-electrolyte interphase growth by elementary reaction kinetics

Yuanyuan Xie, Jianyang Li, Chris Yuan*

Department of Mechanical Engineering, University of Wisconsin Milwaukee, Wisconsin 53211, USA

HIGHLIGHTS

- A pseudo two dimensional multi-physics lithium ion battery model is developed.
- The elementary reaction based SEI layer generation is simulated.
- The battery multi-transport processes are coupled with SEI formation.
- The battery capacity fading processes are studied under different operating conditions.

ARTICLE INFO

Article history:
Received 20 July 2013
Received in revised form
5 September 2013
Accepted 13 September 2013
Available online 24 September 2013

Keywords:
Multiphysics
Lithium ion battery
Modeling
SEI

ABSTRACT

A pseudo two-dimensional mathematical model is developed for a lithium ion battery, integrating the elementary reaction based solid-electrolyte interphase (SEI) growth model with multiple transport processes. The model is validated using the experimental data. Simulation results indicate that the operating temperature has great effect on the SEI layer generation and growth. Under different charging −discharging rates, it is found that high charging−discharging rate can intensify the battery capacity fading process. Different cooling conditions are then applied and show that enhanced surface convective cooling condition can effectively slow down the battery capacity fading. After that, the effect of electrolyte salt concentration and exchange current density are studied. It is found that raising the electrolyte salt concentration can improve the diffusion property of lithium ions, and stabilize the battery performance under lithium ion consumption induced resistance rising. It also suggests that improving exchange current density could greatly decrease the lithium ion battery capacity fading.

Published by Elsevier B.V.

1. Introduction

The rechargeable lithium ion battery is one of the most popular energy storage devices for its high energy density, low energy-weight ratio, small self-discharging and environmental suitability [1]. These beneficial properties as well as low costs have established the rechargeable lithium ion battery as a promising candidate for the next generation automotive and aerospace applications [2]. However, during the charging−discharging cycles or the storage at elevated temperature conditions, lithium ion batteries typically exhibit capacity fading process.

Numerous capacity fading mechanisms of lithium ion battery have been proposed, including electrolyte decomposition, active material degradation, surface film formation, overcharging, self-discharging, and phase change. It is believed that the irreversible capacity loss during the first few charge−discharge cycles is primarily due to the formation of a passivating film on the negative electrode surface [3,4]. This so-called solid electrolyte interphase layer (SEI) is formed at the first time when the electrode contracts the electrolyte solvent [5]. It can isolate the negative electrode from the electrolyte solvent and minimize further reduction reactions of electrolyte components, through which the lithium ions are transported by vacancies and interstitials to reach the active electrode. Typically, the SEI consists of two distinct layers: an inorganic layer and an organic layer. The inorganic layer is a compact layer. It is close to the electrode and in several nanometers thick. The organic layer is a porous layer and on the electrolyte side, which is usually on the order of hundred nanometers thick [6]. The SEI formation can act as a barrier to prevent the electrolyte solvent cointercalation, but the excessive SEI formation may lead to undesirable lithium ions consumption and active electrode area reducing, which finally causes irreversible capacity fading. Experimental studies [7] indicated that the selection of electrolyte solvent and electrode structure could

* Corresponding author. Tel.: +1 414 229 5639; fax: +1 414 229 6958.
E-mail address: cyuan@uwn.edu (C. Yuan).

0378-7753/$ – see front matter Published by Elsevier B.V.
http://dx.doi.org/10.1016/j.jpowsour.2013.09.059

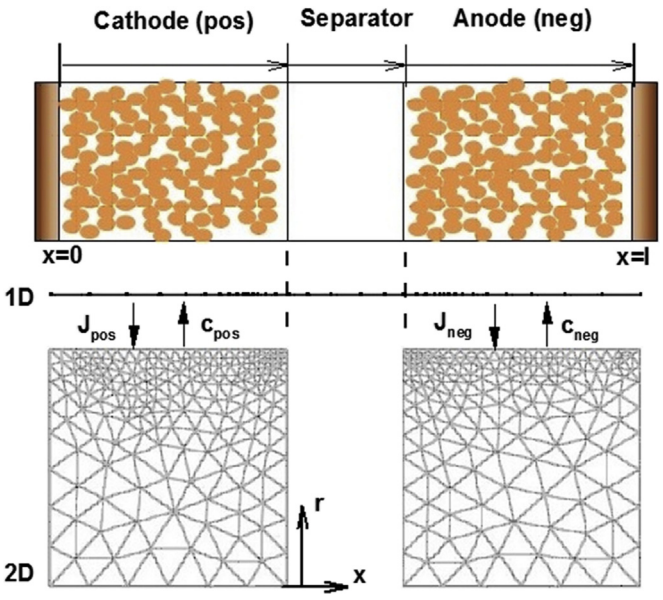

Fig. 1. Physical base and modeling approach.

have crucial effect on the formation and composition of SEI layer. Besides, during the charging–discharging cycles, the operating conditions of lithium ion battery also have been proved to play a very important role on the SEI layer growth and repair [8–10]. Due to the experimental works cannot fundamentally understand these multi-physics processes, modeling approach, as an important complementary, may provide significant advantages to reduce the experimental efforts through exploring the battery performance under different operating conditions.

In literature, various mathematical models have been proposed to reveal the formation and growth of the SEI layer [11–17]. Based on the assumption that the diffusion of electrons through the SEI layer is the rate-determining step, the parabolic law models were developed by Peled [11], Broussely et al. [12] and Ramadass et al. [13], where the side reactions were assumed to occur on the interface between SEI layer and electrolyte. Instead of assuming electron diffusion is rate-determining, Ploehn et al. [14] proposed a SEI formation model by considering the diffusion of solvent through the SEI porous layer as the rate-determining step, of which the numerical results match with the experimental observations fairly well. To study the detailed surface chemistry of SEI layer formation, elementary reaction mechanism was proposed by Aurbach et al. [15], and the reaction based SEI growth models were developed by Christensen et al. [16] and Colclasure et al. [17]. These models all focused on the SEI layer formation process while the battery level models are simplified. Since the lithium ion battery performance highly depends on the operating conditions, it is needed to couple the SEI growth model with the battery level model, so that it can provide more accurate prediction for the battery cycling behavior and the associated processes. However, few such kind multi-physics models [18–22] recently have been presented. Cai et al. [18] incorporated the energy conservation into a multi-physics lithium ion battery life model without the effect of SEI growth. Vazquez-Arenas et al. [19] combined the SEI induced capacity fading model with lithium ion battery model and studied thermal effects on the cycling process. Awarke et al. [20] also proposed a multi-physics model by coupling the electron-diffusion determined SEI growth model with lithium pouch cell model. However, none of them has considered the complicate reaction mechanisms during SEI layer formation. Since the detailed chemistry of SEI formation is critical to study lithium ions intercalation and transport in the electrolyte solution, the objective of this paper is to develop a multi-physics lithium ion battery fading model by coupling the elementary reaction kinetics of SEI layer formation.

In this study, a pseudo two dimensional mathematical model of lithium ion battery is developed, which has bridged multi-physical transport processes with elementary reaction based SEI growth model in a coherent way. Comprehensive simulation studies are performed to investigate the effect of various operating conditions on the battery output performance and capacity fading process.

2. Mathematical model

A lithium ion coin cell has been utilized as the physical base of the developed mathematical model in this paper. Fig. 1 shows the schematic illustration of its structure, which consists of a negative electrode (Li_xC_6), a separator, a positive electrode ($Li_yMn_2O_4$) and two current collectors on the electrode ends. The electrolyte solution is 1 M $LiPF_6$ in a mixture of ethylene carbonate (EC) and dimethyl carbonate (DMC) with the volume fraction ratio of 1:2. The proposed reaction mechanisms of passive film formation on the negative electrode have indicated that the inorganic products, lithium carbonate (Li_2CO_3), is one of the major passive film composition [15]. Although the experimental studies showed that SEI layer could also be formed on positive electrode [16,23], our following mathematical model would only consider its effect on graphite negative electrode. The governing equations of the model include elementary reactions and multi-physics transport processes.

2.1. Elementary reaction kinetics

According to Aurbach [15] and Newman [16], the elementary reaction steps of Li_2CO_3 formation can be simplified as following,

1) The adsorption–desorption reactions:

$$Li^+ + S \rightleftharpoons Li^+_{(s)} \quad (r1)$$

$$EC + S \rightleftharpoons EC_{(s)} \quad (r2)$$

$$C_2H_4 + 2S \rightleftharpoons C_2H_{4(s)} \quad (r3)$$

2) The film formation reaction:

$$CO^{2-}_{3(s)} + 2Li^+_{(s)} \rightleftharpoons Li_2CO_3 + 3S \quad (r4)$$

3) The charge transfer reactions:

$$EC^-_{(s)} \rightleftharpoons EC_{(s)} + e^- \quad (r5)$$

$$C_2H_{4(s)} + CO^{2-}_{3(s)} \rightleftharpoons EC^-_{(s)} + e^- + 2S \quad (r6)$$

where, the subscript (s) stands for the adsorbed species, S is the available surface site. The forward and backward reaction rate coefficients, k_f and k_b, are listed in Table 1. The net reaction rate r_n can be determined as,

$$r_n = k^n_f \prod_i \left[c_i^{\mathrm{Rct}}\right]^{s_i} - k^n_b \prod_i \left[c_i^{\mathrm{Prd}}\right]^{s_i} \quad (1)$$

and the elementary kinetic description of charge transfer can be formulated by Butler–Volmer expression,

Table 1
Elementary reaction rates.

Reaction rate	k_f ($m^3\ mol^{-1}\ s^{-1}$)	k_b ($m^3\ mol^{-1}\ s^{-1}$)
r1	10^8	9×10^{14}
r2	10^{13}	10^8
r3	10^8	10^8
r4	10^{28}	10^{-17}
r5	10^{11}	10^{11}
r6	10^8	10^8

$$J_s = S_j zF\left\{k_f^s\prod_i c_i^{\mathrm{Rct}}\exp\left(\frac{z\alpha_j^a F}{RT}\eta_s\right) - k_b^s\prod_i c_i^{\mathrm{Prd}}\exp\left(-\frac{z\alpha_j^c F}{RT}\eta_s\right)\right\} \tag{2}$$

$$\eta_s = \phi_1 - \phi_2 - U_s^{\mathrm{ref}} - \frac{J_j}{S_{\mathrm{neg}}}R_f, \quad j = \mathrm{neg},\ \mathrm{pos} \tag{3}$$

where, c_i^{Rct} and c_i^{Prd} are the concentration of reactant and product respectively; s_i is the stoichiometric coefficient; S_j is the specific interfacial area; U_s^{ref} is the reference open circuit potential; R_f is the film resistance which is composed of initially formed SEI layer resistance ($R_{f,\mathrm{ini}}$) and produced film resistance during charging–discharging cycles ($R_f(t)$),

$$R_f = R_{f,\ \mathrm{ini}} + R_f(t) \tag{4}$$

$$R_f(t) = \frac{L(t)}{\kappa_p} \tag{5}$$

According to Ploehn et al. [14], the diffusion rate-determining passive film thickness $L(t)$ can be analytically given by,

$$L(t) = 2\lambda\sqrt{D_S^0\exp\left(-\frac{E_a}{RT}\right)t} \tag{6}$$

here, D_S^0 is the Arrhenius diffusion constant; E_a is the activation energy of the diffusion process; λ is implicit solution of

$$\lambda = \frac{c_{\mathrm{Li^+}}}{\sqrt{\pi}c_{\mathrm{Li_2CO_3}}}\frac{\exp\left(-\lambda^2\right)}{\mathrm{erf}(\lambda)} \tag{7}$$

2.2. Transport processes

In addition to elementary reactions, lithium ion battery also includes very complicated transport processes, such as mass diffusion process, charge transport through both solid material and liquid electrolyte, as well as heat transfer. The mass and charge transport processes are coherently coupled together at the active sites of electrodes. To elucidate these complicated interactions, the multi-transport processes are further modeled.

2.2.1. Charge balance

The charge balance includes the charge transport processes in solid phase and liquid phase, which can be formulated using generic Ohm's law,

Solid phase:

$$C_{1,j}\frac{\partial\left(\phi_{1,j}-\phi_{2,j}\right)}{\partial t} + \frac{\partial}{\partial x}\left(-\sigma_j^{\mathrm{eff}}\frac{\partial\phi_{1,j}}{\partial x}\right) = S_j F J_j \tag{8}$$

Liquid phase:

$$C_{2,j}\frac{\partial\left(\phi_{2,j}-\phi_{1,j}\right)}{\partial t} + \frac{\partial}{\partial x}\left(-\kappa_j^{\mathrm{eff}}\frac{\partial\phi_{2,j}}{\partial x}\right) + \frac{2RT\left(1-t_+^0\right)}{F}\frac{\partial}{\partial x}\left(\kappa_j^{\mathrm{eff}}\frac{\partial(\ln c_j)}{\partial x}\right) = S_j F J_j \tag{9}$$

where, $C_{1,j}$ and $C_{2,j}$ are local capacitances; $\phi_{1,j}$ and $\phi_{2,j}$ are the potentials in solid phase and liquid phase respectively; t_+^0 is the transference number of lithium ion; σ_j^{eff} and κ_j^{eff} are the effective conductivities and given by Ref. [18],

$$\sigma_j^{\mathrm{eff}} = \sigma_j(1-\varepsilon_j-\varphi_j) \tag{10}$$

$$\kappa_j^{\mathrm{eff}} = 10^{-4}\times c_j\Big(-10.5+0.668\times10^{-3}c_j+0.494\times10^{-6}c_j^2 +0.074T-1.78\times10^{-5}c_jT-8.86\times10^{-10} c_j^2T-6.96\times10^{-5}T^2+2.80\times10^{-8}c_jT^2\Big)^2\varepsilon_j^{\mathrm{brugg}_j} \tag{11}$$

where, ε_j is the porosity and φ_j stands for the volume fraction.

The local volumetric exchange current can be defined as the summation of Li/Li^+ intercalation process (J_j') and film formation process (J_s),

$$J_j = J_j' + J_{s,\mathrm{neg}} \tag{12}$$

$$J_j' = S_j i_j^0\left\{\exp\left(\frac{z\alpha_j^a F}{RT}\eta_j\right) - \exp\left(-\frac{z\alpha_j^c F}{RT}\eta_j\right)\right\} \tag{13}$$

$$\eta_j = \phi_1 - \phi_2 - U_j - \frac{J_j}{S_{\mathrm{neg}}}R_f \tag{14}$$

Where, U_j is the temperature dependent electrode open circuit potential, and can be approximated by Refs. [18,24],

$$U_j = U_j^{\mathrm{ref}} + \left(T - T_{ref}\right)\frac{\mathrm{d}U_j}{\mathrm{d}T} \tag{15}$$

and the exchange current density i_j^0 is given by,

$$i_j^0 = k_j\left(c_{s,j}^{\max} - c_{s,j}^{\mathrm{surf}}\right)^{\frac{1}{2}}c_{s,j}^{\mathrm{surf}\frac{1}{2}}c_j^{\frac{1}{2}} \tag{16}$$

In the modeling, the potential of solid phase on the negative electrode is set to be zero, while on the surface of positive electrode, the current density equals to the applied value I_0,

$$-\sigma_{\mathrm{pos}}^{\mathrm{eff}}\frac{\partial\phi_{1,j}}{\partial x} = I_0 \tag{17}$$

Since only electrons are transported through the outside load circle, the charge flux of Li ions on two electrode ends is zero,

$$-\kappa_j^{\mathrm{eff}}\frac{\partial\phi_{2,j}}{\partial x}\bigg|_{x=0,l} = 0 \tag{18}$$

2.2.2. Mass balance

The mass balance of lithium ions contains two parts: the mass transfer in solid material and in the liquid electrolyte. In the solid

phase, the mass transfer can be formulated by the Fick's second law based on a spherical particle model,

$$\frac{\partial c_j^s}{\partial t} = D_j^s \frac{1}{r^2}\frac{\partial}{\partial r}\left(r^2 \frac{\partial c_j^s}{\partial r}\right) \tag{19}$$

where, c_j^s is the lithium ion concentration, D_j^s is its diffusion coefficient in solid materials. Due to the electrochemical reaction taking place on the particle surface, the consumption/generation of Li ions can be formulated by,

$$-D_j^s \frac{\partial c_j^s}{\partial r}\bigg|_{r=R_{s,j}} = J_j \tag{20}$$

But at the particle center, the diffusion flux is zero,

$$-D_j^s \frac{\partial c_j^s}{\partial r}\bigg|_{r=0} = 0 \tag{21}$$

In the liquid electrolyte, the material balance of Li ions is given by,

$$\varepsilon_j \frac{\partial c_j}{\partial t} = \frac{\partial}{\partial x}\left(D_j^{\text{eff}} \frac{\partial c_j}{\partial x}\right) + \left(1 - t_+^0\right) a_j J_j - r_1 \tag{22}$$

where, D_j^{eff} is the effective diffusion coefficient [24],

$$D_j^{\text{eff}} = 10^{-8.43-\left(54/\left(T-229-0.005c_j\right)\right)-0.00022c_j} \varepsilon_j^{\text{brugg}_j} \tag{23}$$

The mass transport for other species i is given by,

$$\varepsilon_j \frac{\partial c_{i,j}}{\partial t} = \frac{\partial}{\partial x}\left(D_j^{\text{eff}} \frac{\partial c_{i,j}}{\partial x}\right) + \sum_i s_i r_i \tag{24}$$

Since the mass flux is zero at the two end surfaces of battery, the boundary conditions are applied as,

$$-D_j^{\text{eff}} \frac{\partial c_j}{\partial x}\bigg|_{x=0,l} = 0 \tag{25}$$

2.2.3. Energy balance

The energy balance in lithium ion battery can be formulated by,

$$\rho C_p \frac{\mathrm{d}T}{\mathrm{d}t} = \lambda \frac{\partial^2 T}{\partial x^2} + Q_{\text{rxn}} + Q_{\text{rev}} + Q_{\text{ohm}} \tag{26}$$

where, C_p is the specific heat capacity; λ is the heat conductivity; Q_{rxn} is the total reaction heat generation rate, Q_{rev} is the total reversible heat generation rate, Q_{ohm} is the total ohmic heat generation rate, which are defined by Refs. [18,24],

$$Q_{\text{rxn}} = S_j F J_j \left(\phi_{1,j} - \phi_{2,j} - U_j - \frac{J_j}{S_{\text{neg}}} R_f\right) \tag{27}$$

$$Q_{\text{rev}} = S_j F J_j T \frac{\partial U_j}{\partial T} \tag{28}$$

$$Q_{\text{ohm}} = \sigma_{\text{eff}}\left(\frac{\partial \phi_1}{\partial x}\right)^2 + \kappa_{\text{eff}}\left(\frac{\partial \phi_2}{\partial x}\right)^2 + \frac{2\kappa_{\text{eff}} RT}{F}\left(1 - t_+^0\right)\frac{\partial(\ln c)}{\partial x}\frac{\partial \phi_2}{\partial x} \tag{29}$$

Table 2
Operating parameters.

	Value	Units
Positive electrode thickness	2×10^{-4}	m
Separator thickness	5×10^{-5}	m
Negative electrode thickness	1×10^{-4}	m
Gas constant	8.314	J mol^{-1} K^{-1}
Faraday's constant	96,485	C mol^{-1}
Anode particle radius	1.25×10^{-5}	m
Cathode particle radius	8×10^{-6}	m
Li-diffusivity in anode solid phase	3.9×10^{-14}	m^2 s^{-1}
Li-diffusivity in cathode solid phase	1×10^{-13}	m^2 s^{-1}
Bruggeman coefficient	1.5	1
Cationic transport number	0.363	1
Volume fraction of anode solid phase	0.3	1
Volume fraction of cathode solid phase	0.47	1
Applied 1C charge–discharge current	1.75	A m^{-2}
Initial electrolyte salt concentration	2000	mol m^{-3}
Anode solid phase conductivity	3.8	S m^{-1}
Cathode solid phase conductivity	100	S m^{-1}
Charging/discharging duration	3000	s
Anode local capacitance	3.5×10^{-1}	F
Cathode local capacitance	3.3×10^{-3}	F

Assuming the electrode surface is exposed to the ambient air, the convective heat transfer process is applied on the electrode surface,

$$-\lambda \frac{\partial T}{\partial x}\bigg|_{x=0,l} = h(T_0 - T) \tag{30}$$

3. Solution algorithm and model validation

The mathematical model is solved using COMSOL MULTIPHYSICS V4.3. Two submodel geometries are applied: a one-dimensional lithium ion battery model and a two-dimensional electrode solid phase model. As shown in Fig. 1, the 1D battery model consists of a positive electrode, a separator and a negative electrode, while the 2D solid phase model contains two squares to stand for the solid phase in two electrodes respectively. The vertical coordinate of 2D model stands for the radial direction of a spherical particle while on the horizontal direction the lithium ions diffusion is assumed to be negligible. The concentration of lithium ions is obtained in the 2D solid phase model, and coherently coupled with the multi-physics transport and reaction processes in the 1D battery model. The "extrusion coupling variables" of COMSOL are utilized [18].

The developed model is first calibrated using battery surface temperature curve. The operating parameters are listed in Table 2. As shown in Fig. 2, when the surface convective heat transfer coefficient is set at 23.5 W m^{-2} K^{-1}, the numerical results match with the experimental data reasonably well. Then, we apply 23.5 W m^{-2} K^{-1} on the battery surface and simulate the battery discharging process on the first cycle, the model predictions also match with the experimental data fairly well. The developed mathematical model thus can be used for further numerical studies.

4. Results and discussion

4.1. SEI layer growth

The SEI layer generation process is greatly affected by the applied electrode material and electrolyte solvent, as well as the variation of battery operating conditions [16]. Since the composition of electrodes and electrolyte solvent are definitely known,

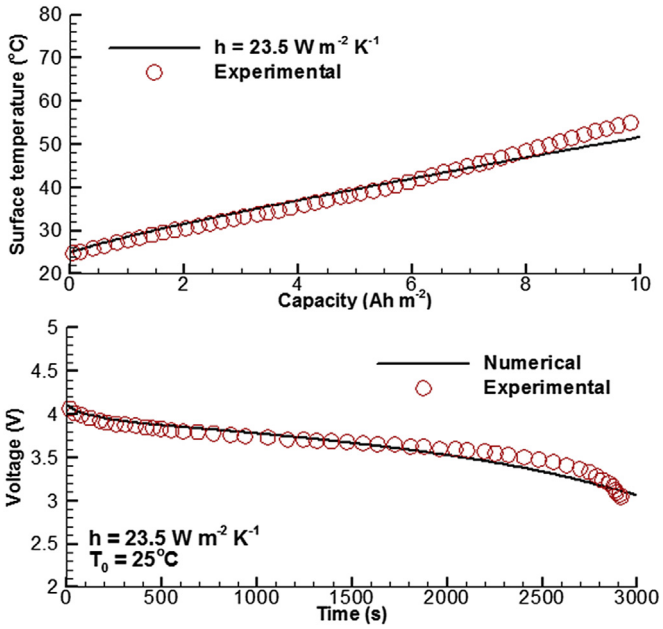

Fig. 2. Comparison between numerical results and experimental data.

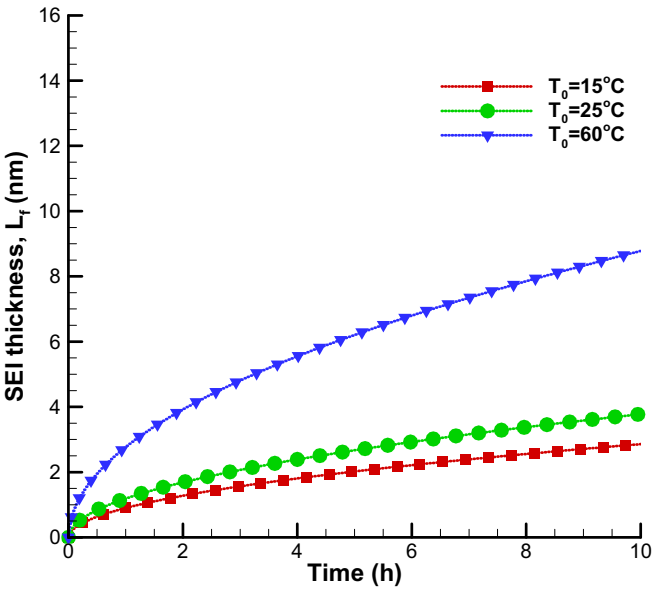

Fig. 3. SEI film growth under different initial operating temperature.

the effect of different operating conditions become more important, one of which is the operating temperature. Fig. 3 has simulated its effect on the SEI layer growth. Three initial temperature conditions of 15 °C, 25 °C and 60 °C are applied and the battery discharge/charge rate is set at 1C. Numerical results show that the thickness of SEI film keeps increasing when battery is operating, and a higher initial operating temperature clearly leads to the generation of a thicker SEI film. Compared with the electrochemical analysis of Christensen et al. [16], the predicted SEI film growth is a little slower. This may be because our model has considered the effect of multi transport processes in lithium ion battery as well as the electrode microstructures. Since SEI layer growth can cause undesirable lithium ions consumption and resistance rising, in the following sections we will study this effect on the global cell performance under different operating conditions.

4.2. Effect of charging–discharging rate

The charging–discharging rate has significant effects on the multi-physics transport processes of lithium ion battery. Three charging–discharging rates of 1C, 0.75C and 0.5C are studied in Fig. 4. The initial operating temperature is set at 25 °C. As shown in Fig. 4(a), the cell capacity of 0.5C case is much higher than the other two cases at the same cell voltage on the first cycle. It can hold around 14 Ah m^{-2} at 3.7 V while that of 1C case can only achieve 7 Ah m^{-2}. This is due to high charging–discharging current density can intensify the electrochemical reactions as well as the SEI layer generation reaction, and lead to the rising of cell polarization resistance. Fig. 4(b) illustrates their effects on the battery cycling performance, where both the charging and discharging period are set to be 3000 s. Upon three current conditions, the voltage drops during discharging process are all kept increasing. Moreover, it shows that the fading trend of 1C case is much worse than the other two. This observation indicates that high charging–discharging rate can greatly intensify the SEI growth induced capacity fading process during battery cycle operating.

4.3. Effect of cooling condition and initial operating temperature

The effect of different cooling conditions on the cell temperature variation is shown in Fig. 5. The discharge current rate is 1C and the initial operating temperature is set at 25 °C. Obviously, the cell surface temperature keeps rising during the discharging process. When the surface convective heat transfer coefficient is increased from zero (insulation boundary) to 50 W m^{-2} K, the cell temperature ascending trend is clearly restrained. It is decreased from as high as 75 °C to around 35 °C at 10 Ah m^{-2}.

Since cooling condition induced temperature variation is significant, Fig. 6 has illustrated its effect on the battery capacity fading, where the discharging/charging rate is set at 1C and the discharging and charging period are both 3000 s. Two convective heat transfer boundary conditions of $h = 0$ W m^{-2} K (insulation) and $h = 23.5$ W m^{-2} K are compared in Fig. 6(a). As shown, the battery capacities of both two cases keep reducing from the 1st cycle to 9th cycle, but it is obvious that the capacity fading of insulation boundary case is much faster than the better cooling one. It means that well convective cooling condition can effectively slow down the lithium ion battery capacity fading process. Similarly, the effect of initial operating temperature on the capacity fading at 9th cycle is studied in Fig. 6(b). It shows the higher operating temperature is applied, the faster fading process will be generated.

4.4. Effect of electrolyte salt concentration

The electrolyte salt concentration is another important factor determining lithium ion battery performance. In Fig. 7, the concentration profiles of the binary electrolyte salt in discharging process at different cycles are simulated. The initial operating temperature is set at 25 °C and the discharge current rate is 1C. It shows the electrolyte concentration profile of 6th cycle is much flatter than that of other cycles, which suggests that the diffusion property of electrolyte solvent on 6th cycle is better. This is because more heat will be generated as the charge–discharge cycle goes on, which can benefit the diffusion process. Besides, it can be noticed that the concentration profile patterns of 6th cycle and 4th cycle are very close. Because the SEI layer thickness keeps increasing during

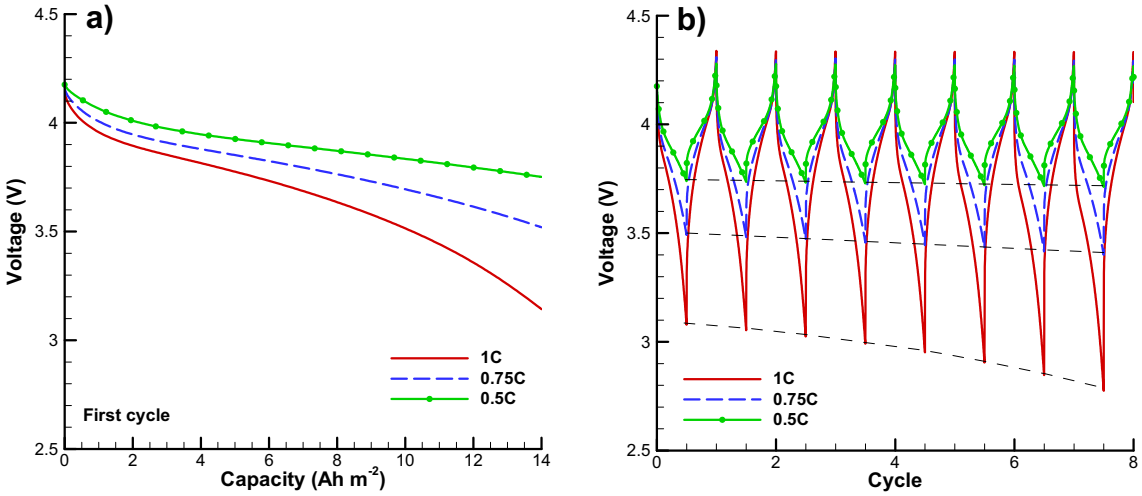

Fig. 4. Effect of charging–discharging rate on the battery charging–discharging cycle performance.

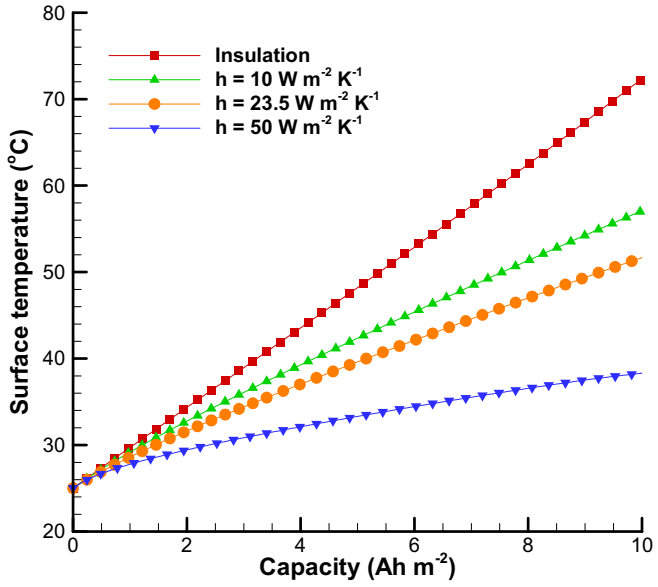

Fig. 5. Surface temperature profiles under different cooling conditions.

the cell operating, this observation suggests its passive effect on the electrolyte solvent diffusion/reaction is also increasing.

According to the elementary reaction mechanism, the step reaction rates are determined not only by the applied battery operating conditions but also by the concentration of each reactant. Fig. 8 illustrates the effect of different initial electrolyte salt concentration on the capacity fading of lithium ion battery, where three concentrations of 0.001 mol cm^{-3}, 0.002 mol cm^{-3} and 0.004 mol cm^{-3} are employed respectively. The initial temperature is 25 °C and other operating conditions are the same as above cases. The battery discharging performances are compared at the 4th cycle. It can be seen that the battery with 0.004 mol cm^{-3} electrolyte salt has the slowest fading process. This can be explained by that adding more lithium ions to the battery electrolyte solvent can improve the diffusion property, and stabilize the cell performance under lithium ion consumption induced resistance rising. Besides, different cooling methods on three electrolyte cases are also compared in Fig. 8, which shows that enhanced cooling condition can obviously slow down their capacity fading process.

4.5. Effect of exchange current density

Theoretically, the exchange current is the ongoing current of a redox reaction in both cathodic and anodic directions, which

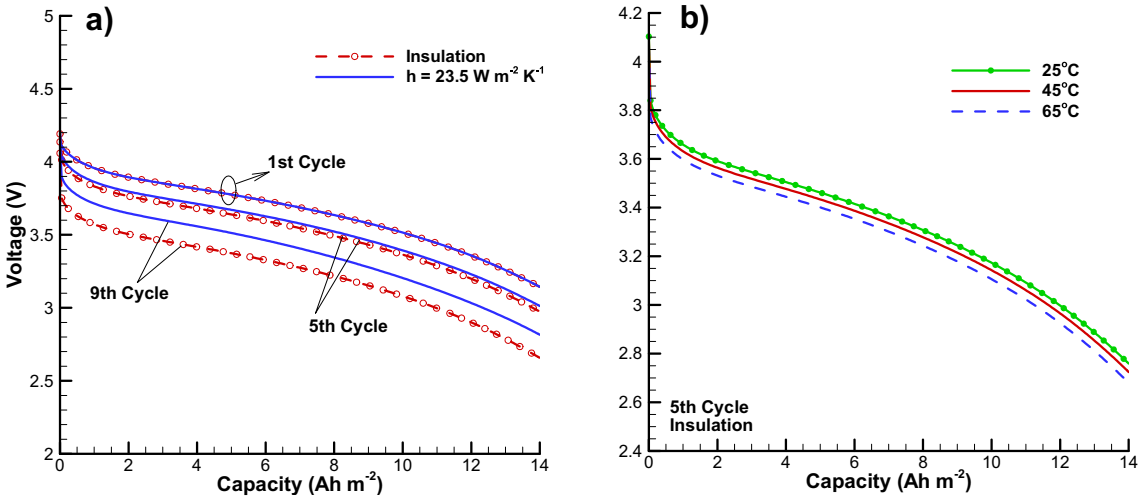

Fig. 6. Effect of a) different cooling conditions and b) initial operating temperature on the battery capacity fading process.

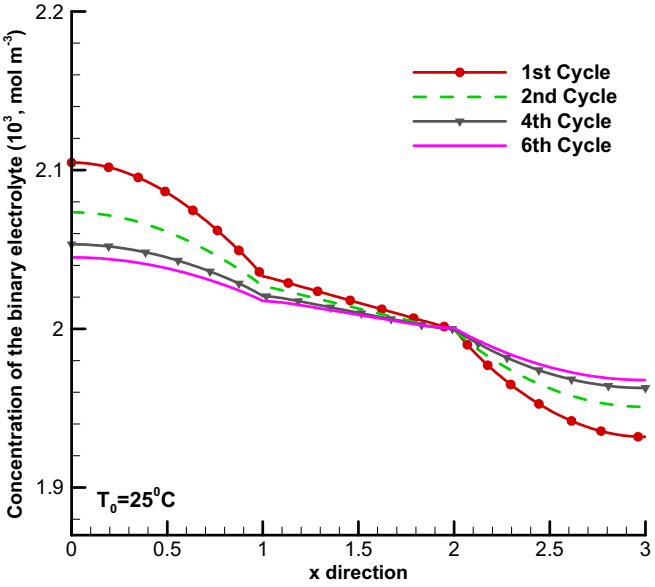

Fig. 7. The concentration profile of the binary electrolyte salt in different cycles during discharging process.

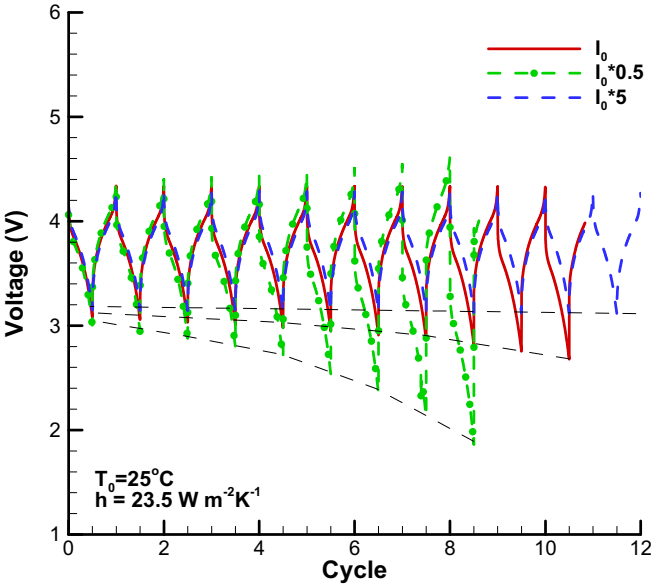

Fig. 9. Effect of exchange current density on the battery capacity fading process.

reflects the intrinsic rates of electrochemical processes. It depends critically on the nature of the electrodes and electrolyte solvent including the physical structure, chemical composition and the electrochemical properties. Since it has great influence on the cell performance, Fig. 9 has illustrated different exchange current conditions during the battery cycle operating. To make a comparison, the exchange current densities are chosen to be 50% and 5 times of its base value respectively. The cycle process is simulated at 25 °C and 1C charge/discharge rate. It is clear that the lowest exchange current density case (0.5 I_0) has the fastest fading process. Since the exchange current density reflects the electrochemical reaction rate, it can be concluded that the method like increasing the active surface area, raising Li ion concentration that can intensify the electrochemical reactions could have positive effect to slow down the SEI growth induced battery fading process.

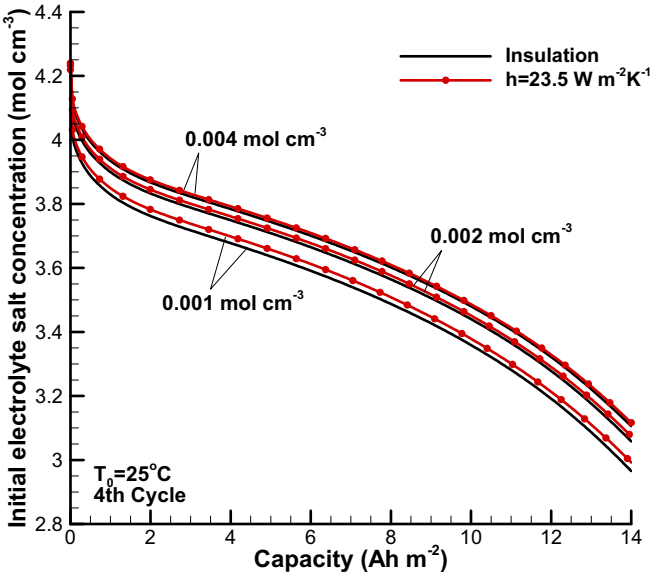

Fig. 8. Effect of binary electrolyte salt concentration on the battery capacity fading process.

5. Conclusion

A pseudo two-dimensional mathematical model of lithium ion battery is developed by coherently coupling the multi-physics transport processes with elementary reaction based SEI growth model. The model is validated with experimental data. Simulation results indicate that the operating condition of lithium ion battery has significant influence on the SEI layer generation. Under different charging–discharging rate, the comparison study shows that high charging–discharging rate can greatly intensify the battery capacity fading process. With changing surface cooling condition, the numerical results also show that well convective cooling condition can effectively slow down the battery capacity fading. The battery performances of three different electrolyte salt concentrations are then simulated, which suggests raising the electrolyte salt concentration can improve the diffusion property of lithium ions, and stabilize the cell performance under lithium ion consumption induced resistance rising. The effect of exchange current is finally simulated. It is found that the method of raising exchange current like increasing the active surface area or raising Li ion concentration could slow down the battery fading process through intensifying the electrochemical reactions.

Acknowledgments

The authors gratefully acknowledge the financial support from UWM Research Growth Initiative (RGI).

List of symbols

$c_i^{\mathrm{Rct}}, c_i^{\mathrm{Prd}}$	the concentration of reactant and product
C_p	the specific heat capacity
D_i^{eff}	the effective diffusion coefficient
D_S^0	Arrhenius diffusion constant
E_a	the activation energy of the diffusion process
F	the Faraday's constant

i_j^0	the exchange current density
I_0	the applied charging–discharging current density
J_j	the local volumetric exchange current
k_f, k_b	forward and backward reaction rate coefficients
R_f	the film resistance
s_i	stoichiometric coefficient
S_j	the specific interfacial area
t_+^0	the transference number of lithium ion
U_j	the electrode-open circuit potential
U_s^{ref}	the reference open circuit potential
$\phi_{1,j}$, $\phi_{2,j}$	the potentials in solid phase and liquid phase
σ_j^{eff}, κ_j^{eff}	the effective conductivities
λ	the heat conductivity

References

[1] V. Ramadesigan, P.W.C. Northrop, S. De, S. Santhanagopalan, R.D. Braatz, V.R. Subramanian, J. Electrochem. Soc. 159 (3) (2012) R31–R45.
[2] L. Lu, X. Han, J. Li, J. Hua, M. Ouyang, J. Power Sources 226 (2013) 272–288.
[3] E. Peled, D. Golodnitsky, G. Ardel, J. Electrochem. Soc. 144 (8) (1997) L208–L210.
[4] D. Aurbach, B. Markovsky, M.D. Levi, E. Levi, A. Schechter, M. Moshkovich, Y. Cohen, J. Power Sources 95 (1999) 81–82.
[5] M. Nie, D. Chalasani, P.D. Abraham, J. Phys. Chem. C 177 (3) (2013) 1257–1267.
[6] A.M. Andersson, A. Henningson, H. Siegbahn, U. Jansson, K. Edstrom, J. Power Sources 119 (2003) 522–527.
[7] P. Verma, P. Maire, P. Novak, Electrochim. Acta 55 (2010) 6332–6341.
[8] J. Yan, J. Zhang, Y.C. Su, Electrochim. Acta 55 (5) (2010) 1785–1794.
[9] L. Zhao, I. Watanabe, T. Doi, J. Power Sources 161 (2) (2006) 1275–1280.
[10] M. Zheng, Q. Dong, H. Cai, J. Electrochem. Soc. 152 (11) (2005) A2207–A2210.
[11] E. Peled, J. Electrochem. Soc. 126 (1979) 2047.
[12] M. Broussely, S. Herreyre, P. Biensan, P. Kasztejna, K. Nechev, R.J. Staniewicz, J. Power Sources 97 (2001) 13–21.
[13] P. Ramadass, B. Haran, P.M. Gomadam, R. White, B.N. Popov, J. Electrochem. Soc. 151 (2) (2004) A196–A203.
[14] H.J. Ploehn, P. Ramadass, R.E. White, J. Electrochem. Soc. 151 (3) (2004) A456–A462.
[15] D. Aurbach, B. Markovsky, I. Weissman, E. Levi, Y.E. Eli, Electrochim. Acta 45 (1999) 67–86.
[16] J. Christensen, J. Newman, J. Electrochem. Soc. 151 (11) (2004) A1977–A1988.
[17] A.M. Colclasure, K.A. Smith, R.J. Kee, Electrochim. Acta 58 (2011) 33–43.
[18] L. Cai, R.E. White, J. Power Sources 196 (2011) 5985–5989.
[19] J.V. Arenas, M. Fowler, X. Mao, S. Chen, J. Power Sources 215 (2012) 28–35.
[20] A. Awarke, S. Pischinger, J. Ogrzewalla, J. Electrochem. Soc. 160 (1) (2013) A172–A181.
[21] P.M. Gomadam, J.W. Weidner, R.A. Dougal, R.E. White, J. Power Sources 110 (2002) 267–284.
[22] S. Rael, M. Hinaje, J. Power Sources 222 (2013) 112–122.
[23] D.P. Abraham, J. Liu, C.H. Chen, Y.E. Hyung, M. Stoll, N. Elsen, S. Maclaren, R. Twesten, R. Haasch, E. Sammann, I. Petrov, K. Amine, G. Henriksen, J. Power Sources 119 (2003) 511–516.
[24] K. Kumaresan, G. Sikha, R.E. White, J. Electrochem. Soc. 115 (2) (2008) A164–A171.